HHS Public Access

Author manuscript

Acta Biomater. Author manuscript; available in PMC 2017 July 06.

Published in final edited form as:

Acta Biomater. 2016 March ; 33: 264–274. doi:10.1016/j.actbio.2016.01.026.

Magnetic induction heating of superparamagnetic nanoparticles during rewarming augments the recovery of hUCM-MSCs cryopreserved by vitrification

Jianye Wang[1], **Gang Zhao**[1,2,*], **Zhengliang Zhang**[3], **Xiaoliang Xu**[4], and **Xiaoming He**[5,*]

[1]Department of Electronic Science and Technology, University of Science and Technology of China, Hefei 230027, China

[2]Anhui Provincial Engineering Technology Research Center for Biopreservation and Artificial Organs, Hefei 230027, China

[3]Anhui Huien Biotechnology Corporation, LTD., Hefei 230088, China

[4]Department of Physics, University of Science and Technology of China, Hefei 230026, China

[5]Department of Biomedical Engineering, The Ohio State University, Columbus, Ohio 43210, USA

Abstract

Cryopreservation by vitrification has been recognized as a promising strategy for long-term banking of living cells. However, the difficulty to generate a fast enough heating rate to minimize devitrification and recrystallization-induced intracellular ice formation during rewarming is one of the major obstacles to successful vitrification. We propose to overcome this hurdle by utilizing magnetic induction heating (MIH) of magnetic nanoparticles to enhance rewarming. In this study, superparamagnetic (SPM) Fe_3O_4 nanoparticles were synthesized by a chemical coprecipitation method. We successfully applied the MIH of Fe_3O_4 nanoparticles for rewarming human umbilical cord matrix mesenchymal stem cells (hUCM-MSCs) cryopreserved by vitrification. Our results show that extracellular Fe_3O_4 nanoparticles with MIH may greatly suppress devitrification and/or recrystallization during rewarming and significantly improve the survival of vitrified cells. We further optimized the concentration of Fe_3O_4 nanoparticles and the current of an alternating current (AC) magnetic field for generating the MIH to maximize cell viability. Our results indicate that MIH in an AC magnetic field with 0.05% (w/v) Fe_3O_4 nanoparticles significantly facilitates rewarming and improves the cryopreservation outcome of hUCM-MSCs by vitrification. The application of MIH of SPM nanoparticles to achieve rapid and spatially homogeneous heating is a promising strategy for enhanced cryopreservation of stem cells by vitrification.

Graphical abstract

[*]Author to whom correspondence should be addressed. ZhaoG@ustc.edu.cn (G.Z.); he.429@osu.edu (X.H.). **Work telephone number:** +8618256929838; +1 614 247 8759.

Disclosure

The authors declare no conflict of interests.

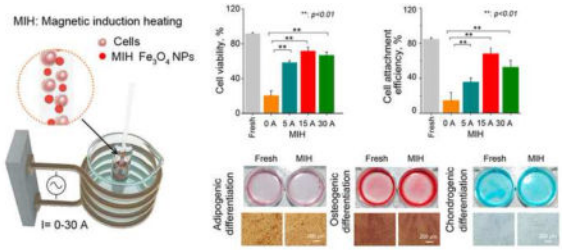

Keywords

Magnetic induction heating; Fe_3O_4 nanoparticles; Cryopreservation; Vitrification; hUCM-MSCs

Introduction

Mesenchymal stem cells (MSCs) show self-renewal and multi-lineage differentiation properties and are important for cell-based therapies to treat a variety of disorders [1–4]. The umbilical cord matrix (UCM), which is routinely discarded after childbirth, is a valuable resource for non-invasive collection of MSCs without any ethical issues [5]. MSCs from human UCM (hUCM-MSCs) are an abundant source of adult stem cells and are an alternative to embryonic stem cells [6, 7]. UCM-MSCs show low immunogenicity and elicit a lower incidence of graft rejection and post-transplant infections compared with other sources of adult stem cells.[8] Thus, hUCM-MSCs are an extremely valuable candidate for cell-based regenerative medicine.[9, 10] Moreover, banking hUCM-MSCs is essential to meet the ever increasing needs of the cells for clinical applications and research [11].

Cell cryopreservation is a technology for long-term storage of cells by cooling the cells to cryogenic temperature with minimal metabolic activities [12–15]. Although it has been commonly used for cell cryopreservation, the conventional slow-freezing approach is time-consuming and usually requires an expensive programmable freezer to achieve the desired cooling rates that are different for different types of cells [16–18]. Vitrification is attracting more and more attention in recent years as a fast and economic alternative to slow freezing, particularly for the cryopreservation of stem cells and reproductive cells [19–23]. Vitrification is a process by which the disordered liquid state of water is brought to a standstill as a solid without crystallization during cooling [24]. High cooling rates and high concentrations (4–8 M) of cryoprotectants have been conventionally used to achieve vitrification. Most research effort has been focused on achieving the ultra-rapid cooling rate and lowering the concentration of cryoprotectant required for vitrification [18, 19, 25–27]. However, due to the low thermal conductivity of biological samples, the conventional approach of rewarming large-volume cryopreserved samples in a water bath is associated with non-uniform distribution of temperature, and this non-uniformity can induce thermal stress that can crack the brittle cryopreserved sample [28–30]. Moreover, a high heating rate for rewarming is crucial, because devitrification and recrystallization will occur if the temperature cannot be rapidly increased above the melting points of the aqueous sample. Therefore, both the heating rate and uniformity of heating during rewarming are important to cryopreservation by vitrification.

Electromagnetic (EM) heating, which produces a higher warming rate and more uniform heating than the conventional water bath rewarming method, is considered to be an effective approach for rewarming cryopreserved samples [31, 32]. Previous studies have been focused on microwave and high frequency RF rewarming (hundreds of MHz even GHz in frequency). Ketterer *et al.* thawed cryopreserved canine kidney using a microwave oven [33, 34]. However, because the microwave penetration depth is limited and a uniform heating may not be achieved, the rewarming outcome was not favorable [35]. Ruggera *et al.* proposed rapid EM heating using a resonant helical coil applicator to prevent the formation of ice crystals during the rewarming for the cryopreservation of cells and organs [36]. Robinson *et al.* further developed this EM heating system with a cylindrical resonance cavity [31, 37]. Gao *et al.* developed a single-mode resonant cavity to achieve rapid and uniform warming of cryopreserved biomaterials [38]. In addition, Jin *et al.* used infrared laser pulses to achieve ultra-rapid warm rates (10,000,000 °C/min) for rewarming frozen or vitrified oocytes [39–41]. However, these approaches need complicated instruments and are time consuming.

Magnetic nanoparticles, which possess several unique characteristics including biocompatibility and SPM properties, are widely applied in medicine [42–45]. They can be rapidly heated upon exposure to an AC magnetic field and are uniformly spread throughout the biomaterial [30, 46]. Heating magnetic nanoparticles can be conveniently realized with an induction apparatus over a medium frequency range (several hundreds of kHz), and has been investigated to treat tumors [42, 43, 46–50]. Magnetic nanoparticles have also been shown to improve the efficiency of the microwave rewarming process, and augment tumor treatment with cryosurgery [51, 52]. However, the effect of magnetic induction heating (MIH) of SPM nanoparticles in an AC magnetic field on vitrified cryopreservation has not been reported. In this study, we synthesize and characterize SPM nanoparticles and apply them, as part of the vitrification solution, for hUCM-MSCs cryopreservation by vitrification. We found that SPM nanoparticles improve the rewarming of hUCM-MSCs cryopreserved by vitrification under an alternating magnetic field.

Materials and methods

Synthesis of Fe_3O_4 nanoparticles

Fe_3O_4 nanoparticles were synthesized by a chemical coprecipitation method detailed elsewhere [53]. In brief, $FeCl_3$ (0.5 mol/L) and $FeSO_4$ (0.5 mol/L) were mixed in water, and aqueous ammonia solution was added into the mixture drop by drop with vigorous stirring until the pH reached 9 under N_2 gas. The mixture was further stirred for 30 min to complete the reaction. Afterward, Fe_3O_4 nanoparticles were collected and washed three times with distilled water by centrifugation and kept in a refrigerator for future use.

Characterization of Fe_3O_4 nanoparticles

The morphology of the Fe_3O_4 nanoparticles were examined using a H-700H transmission electron microscope (TEM, Hitachi, Ltd., Tokyo, Japan) at an accelerating voltage of 100 kV, and the samples of Fe_3O_4 nanoparticles for the TEM study were prepared by placing drops of the nanoparticles in ethanol on the surface of carbon grids. The size of Fe_3O_4

nanoparticles was assessed by dynamic light scattering (DLS) using a DynaPro-MS800 instrument (Wyatt Technology, Santa Barbara, CA, USA), for which the Fe_3O_4 nanoparticles were dispersed in phosphate-buffered saline (PBS) at a concentration of 50 μg/mL. After ultrasonication, the aqueous solution was obtained after the samples were equilibrated at 25 °C for 10 min. The surface zeta potential of Fe_3O_4 nanoparticles was measured using a Malvern Nano-ZS90 Zetasizer Nano instrument (Malvern Instruments Ltd., Malvern, UK) at room temperature. The magnetic properties of the Fe_3O_4 nanoparticles were measured with a vibrating sample magnetometer (VSM, Quantum Design, Inc., San Diego, CA, USA) vibrating sample magnetometer at room temperature.

hUCM-MSC culture

hUCM-MSCs were generously provided by Anhui Huien Biotechnology Corporation, LTD. (Hefei, Anhui, China), and they have been used in previous studies [54, 55]. To isolate the hUCM-MSCs, UCMs from the UCM of consenting patients were enzymatically dissociated in Dulbecco's modified Eagle medium (DMEM) with 0.25% (w/v) trypsin (Gibco, Carlsbad, CA, USA), 300 U collagenase type II (Gibco), and 10% (v/v) fetal bovine serum (FBS, Gibco). After incubating at 37 °C for 60 min, the dissociation was terminated by washing in medium (DMEM with 10% (v/v) FBS), and the samples were sequentially filtered through a 25 μm nylon mesh to remove tissue debris. The isolated hUCM-MSCs were suspended in DMEM containing 10% (v/v) FBS, and cultured at 37 °C and 5% CO_2 in a humidified incubator. Culture medium was changed every other day until reaching 80–90% confluency. All cells used in this study were no more than the third passage.

Cell uptake of Fe_3O_4 nanoparticles

For the cell uptake study, Fe_3O_4 nanoparticles were purified by dialyzing against sterile PBS overnight. The purified Fe_3O_4 nanoparticles were then dispersed in culture medium and incubated with hUCM-MSCs for 12 h at 37 °C and 5% CO_2 in an incubator. Afterward, the hUCM-MSCs were fixed with glutaraldehyde for examination using a Hitachi H-700H TEM (Hitachi, Ltd., Tokyo, Japan) instrument at an accelerating voltage of 80 kV.

The cell uptake of nanoparticles was also studied with a colorimetric assay detailed in a previous study [56, 57]. Briefly, the hUCM-MSCs after incubating with Fe_3O_4 nanoparticles were mixed with 1.2 M HCl and 2 M ascorbic acid at 65–70 °C for approximately 2 h. A reagent containing ferrozine, neocuproine, ascorbic acid, and ammonium acetate was then added. The absorbance of the resultant solution at 562 nm was measured using a Hitachi U2810 UV-Vis spectrophotometer. A standard curve of the absorbance at 562 nm was obtained using Fe_3O_4 nanoparticles at concentrations of 0, 0.1, 0.5, 1.0, 2.0, and 5.0 μg/mL.

Cytotoxicity of Fe_3O_4 nanoparticles

To assess the cytotoxicity of Fe_3O_4 nanoparticles, cell proliferation assay was performed by culturing hUCM-MSCs with the nanoparticles. The hUCM-MSCs were seeded in 96-well plates at a density of 10^5 cells per mL in 100 μl medium. After overnight culture, the medium was replaced with medium containing 0.01%, 0.05%, and 0.1% (w/v) Fe_3O_4 nanoparticles for further culture for up to 3 d. The cells cultured in medium without the nanoparticles were also studied to serve as control. The CCK-8 reagent Kit (Dojindo Inc.,

Kumamoto, Japan) was used to measure cell proliferation. After incubating with cells for 4 h at 37 °C, absorbance at 450 nm was measured to quantify the cell number in each well according to a standard line made with the known number of cells in each well. The proliferation capacity was quantitatively assessed as the relative cell number on day 2 & 3 to that on day 1.

Cryopreservation of hUCM-MSCs

Before cryopreservation, the attached hUCM-MSCs were harvested at 70–80% confluency. The hUCM-MSCs were lightly trypsinized, collected by centrifugation at 500g for 5 min, and resuspended in culture medium (DMEM with 10% (v/v) FBS) for further use. For the vitrification studies, the cells were spun down at 500g for 5 min and resuspended in 1 mL of pre-cooled (on ice for 10 min) culture medium with 1.0 M 1,2-propanediol (PROH, Sigma-Aldrich, St. Louis, MA, USA), 1.0 M Ethylene Glycol (EG, Sigma-Aldrich) and 0.5 M trehalose (Sinozyme Biotechnology Co., Ltd., China). The cells were then collected by centrifuging at 500g for 5 min, resuspended in a pre-cooled vitrification solution made of culture medium with 2.0 M PROH, 2.0 M EG, and 0.5 M trehalose, and equilibrated on ice for another 10 min. Afterward, the cells were mixed with Fe_3O_4 nanoparticles at various concentrations (0.01–0.1% (w/v)) pre-cooled on ice to prevent cellular uptake of the nanoparticles.

As illustrated in Scheme 1, for cryopreservation by vitrification, 200 μL of the cell suspension was then loaded into straws (Figure S1a, FHK, Japan) at a density of 10^7 cells/mL. The straws were immediately cooled by plunging into liquid nitrogen and stored there for 1 day. The cryopreserved sample was rewarmed by plunging the straw into 37 °C culture medium with 0.2 M trehalose under an AC magnetic field generated by a 6-loop coil apparatus (Shenzhen Shuangping Power Supply Technology Co., Ltd., China, Figure S1b) for magnetic induction heating (MIH) at a medium frequency (375 kHz) for 10 s. The cryopreserved sample warmed by plunging the straws into warm culture medium with 0.2 M trehalose without MIH was studied in parallel to serve as negative control. The cell suspension was then unloaded from the straw with a syringe. The Fe_3O_4 nanoparticles were removed from the collected suspension using a ferromagnet. The post-cryopreservation cells were centrifuged at 500g for 5 min and resuspended in medium for evaluation of viability and further culture.

Assessment of cell viability with fluorescence staining

The viability of hUCM-MSCs post-cryopreservation was evaluated using an acridine orange/ethidium bromide (AO/EB) staining kit (KeyGen BioTECH Co., Ltd., China). The cells were resuspended in 20 μL fresh medium and the fluorescence staining solution (1 μL) was added into the cell suspension. The cells were stained with the fluorescent dyes (i.e., AO and EB) by incubating the sample at room temperature for 5 min. Fluorescence images of the cells were then taken using a DS-Ri1 (Nikon, Japan) camera and 10× objective equipped on a Nikon Ti-FL inverted microscope with fluorescence capability. The red (i.e., EB) and green (AO) stained cells in the fluorescence images were counted using Image J (NIH, Bethesda, USA) as the dead and live cells, respectively. The cell viability was further calculated as the percentage of viable cells out of the total (i.e., live and dead) cells counted.

Flow cytometry analysis of cell necrosis and apoptosis

The cell viability of post-cryopreservation also was analyzed by flow cytometry to quantify the cell necrosis and apoptosis. The cells post-cryopreservation were collected and washed in PBS. The cells were then resuspended in binding buffer (0.01 M HEPES pH 7.4, 0.14 M NaCl, and 2.5 mM $CaCl_2$), stained with 5 μL FITC-conjugated Annexin V and 5 μL propidium iodide (PI) (Vazyme Biotech Co., Ltd., China) in 100 μL binding buffer on ice. The PI and Annexin V were used to stain cells that died of necrosis and apoptosis, respectively. The cells were incubated for 15 min in the dark. The stained samples were analyzed using a flow cytometer (BD FACSCalibur, Becton Dickinson, San Jose, CA, USA) together with the Flowjo software.

Analysis of attachment efficiency and proliferation

To further check the long-term viability of cells post-cryopreservation, cell attachment and proliferation were estimated as detailed in a previous study [58]. The hUCM-MSCs post cryopreservation were incubated with fresh culture medium for 10 min at 37 °C and the cells spun down to remove cryoprotective agents. The cells were then further cultured for one day. Fresh hUCM-MSCs without cryopreservation were studied as control. The attachment efficiency was calculated as the ratio of the total number of attached cells post-cryopreservation of a cryopreserved sample to that of the control non-frozen sample at day 1.

To quantify cell proliferation, the cell growth was evaluated over a 3-day period as previously described [59]. The cryopreserved hUCM-MSCs were seeded in 6-well plates. After 1 day of culture, the cells were detached and 1.5×10^4 cells were seeded in 48-well plates. Fresh hUCM-MSCs without cryopreservation were seeded in the same way to serve as control. At different times (1, 2, and 3 d), the medium was removed and the cells washed using PBS twice. The cell number in each well at different times was then determined using the CCK-8 kit and proliferation was calculated as the ratio of the cell number on day 2 and day 3 to the cell number on day 1.

Functional characterization of hUCM-MSCs

For functional study, we checked the stemness and multi-lineage potential of the hUCM-MSCs post cryopreservation. The expression of two surface markers (CD44+ and CD31−) was analyzed by flow cytometry, and the multi-lineage potential of hUCM-MSCs was tested by adipogenic, osteogenic, and chondrogenic differentiation. The fresh and post cryopreserved (treated by induction heating at 15 A, 375 kHz for 10 s) hUCM-MSCs were cultured for 3 d, detached using trypsin/EDTA, washed with PBS, and stained with CD44-FITC (BD Biosciences, San Jose, CA, USA) and CD31-PI (BD Biosciences) antibodies. The stained samples were analyzed using a flow cytometer (BD FACSCalibur). For multi-lineage potential assays, both the fresh and post-cryopreserved hUCM-MSCs were studied using adipogenic, osteogenic, and chondrogenic differentiation kits (Invitrogen, Carlsbad, CA, USA). In the differentiation assays, 2×10^5 cells were seeded in 6-well plates and medium was changed every other day till the cell confluency reached 50%. The supplemented induction medium was added into the 6-well plates for culture, the medium was changed every 3 d, and the cells were cultured for 12 d. The differentiated cells were harvested and

fixed with 4% paraformaldehyde. The fixed cells were stained with Oil Red O, Alizarin Red S, or Alcian Blue for adipogenic, osteogenic, or chondrogenic differentiations, respectively.

Statistical analysis

All data are presented as the mean ± standard deviation from at least three independent runs. The statistical analyses are performed using Student's two-tail paired *t* tests between the groups, and a p value < 0.05 is considered statistically significant. Statistical significance between the mean values of more than two groups is determined using one-way analysis of variance (ANOVA) with Tukey post-hoc tests. The difference is considered statistically significant when the p value is less than 0.05.

Results and discussion

Characterization, cell uptake, and cytotoxicity of Fe_3O_4 nanoparticles

Fe_3O_4 nanoparticles were synthesized using the chemical coprecipitation method and their morphology and size were characterized by TEM (Figure 1a). The nanoparticles are largely spherical with a quite uniform size (10.02 ± 1.56 nm in diameter). The diameter of Fe_3O_4 nanoparticles in aqueous solution (PBS) was determined by DLS to be 25.2 ± 9.3 nm, as shown in Figure 1b. Probably because the nanoparticles have high affinity to water molecules to form a hydration layer on their surface, the diameter determined by DLS is larger than that of TEM. The nanoparticles have a negatively charged surface (−35.0 ± 5.2 mV) at room temperature (Figure 1c). The magnetic property characterization (Figure 1d) shows that Fe_3O_4 nanoparticles have SPM property and high magnetization with a saturation value of 42.69 emu/g for an individual Fe_3O_4 nanoparticle. When the size of Fe_3O_4 nanoparticles is smaller than 30 nm, they exhibit size-dependent SPM behavior [60]. Under an external magnetic field, they become magnetized up to their saturation magnetization and can convert the some of the energy carried by the external magnetic field into heat. Upon removal of the external magnetic field, they no longer exhibit any residual magnetic interaction. Unlike bulk magnetite, SPM nanoparticles, containing a single magnetic domain, exhibits high magnetic susceptibility [61].

Fe_3O_4 nanoparticles can interact with the cell plasma membranes to form endosomes and enter cells [62, 63]. To quantify the cell uptake of Fe_3O_4 nanoparticles, a colorimetric assay for detecting the colored complex formed as a result of the reaction of ferrozine with Fe^{2+} reduced from the Fe_3O_4 nanoparticles [57]. Figure 2a shows the concentration of Fe_3O_4 nanoparticles loaded into the hUCM-MSCs at different incubation times. The uptake increases gradually with the incubation time from 4 to 8 h and reaches a plateau after 8 h. After incubated with hUCM-MSCs for 12 h at 37 °C, the Fe_3O_4 nanoparticles localized in endosomes can be observed by TEM, as shown in Figure 2b. Fe_3O_4 nanoparticles are segregated from the cytoplasm by the membrane of endosome. Moreover, the nucleus, mitochondria, and endoplasmic reticula of hUCM-MSC are distinct, which indicate that the uptake of Fe_3O_4 nanoparticles may not affect the activity of hUCM-MSCs.

To check the toxicity of Fe_3O_4 nanoparticles to hUCM-MSCs, we obtained proliferation of hUCM-MSCs using the CCK-8 kit after incubating the cells with the Fe_3O_4 nanoparticles

for 1, 2, and 3 d. Figure 2c shows the proliferation of hUCM-MSCs after exposure to Fe_3O_4 nanoparticles at different concentration (0, 0.01, 0.05, and 0.1% (w/v)) for 1, 2, and 3 d. Our data show that the Fe_3O_4 nanoparticles at concentrations as high as 0.1% (w/v) do not affect the proliferation of the hUCM-MSCs, even after 3 d of incubation. These results indicate that the SPM Fe_3O_4 nanoparticles do not affect mitochondrial function (checked using a CCK-8 kit) at concentrations as high as 0.1% (w/v). Therefore, Fe_3O_4 nanoparticles are considered as a biocompatible nanomaterial for augmenting the cryopreservation of primary hUCM-MSCs by vitrification.

Effect of Fe_3O_4 nanoparticles on cryopreservation of primary hUCM-MSCs by vitrification

It has been reported that nanoparticles have a significant impact on the thermophysical processes/parameters of cryopreservation such as homogeneous nucleation, phase change temperature, the ice growth and devitrification temperature [64–67]. Hydroxyapatite nanoparticles even can significantly improve the survival rate of *in vitro* matured porcine oocytes post-cryopreservation by vitrification [68]. To detect the effects of Fe_3O_4 nanoparticles on cryopreservation by vitrification, the outcome of vitrification with varying concentration of Fe_3O_4 nanoparticles were investigated. As detailed in the previous studies [20, 26], the appearance of opacity or visible ice formation was considered as non-vitrification. If there is no observable opacity, it is taken as being vitrified. Figure 3a shows a typical picture of the vitrification solution (2.0 M PROH, 2.0 M EG in culture medium) with or without Fe_3O_4 nanoparticles in straws after the straws were plunged into liquid N_2. The solution without the Fe_3O_4 nanoparticles is transparent while, ice formation is evident in the vitrification solution with 0.05% (w/v) Fe_3O_4 nanoparticles. Trehalose is a non-penetrating cryoprotectant and lyoprotectant that has been shown to protect various biologicals from freezing and drying-induced injury [59, 69–72]. When both Fe_3O_4 nanoparticles and trehalose (0.5 M or higher) were incorporated into the vitrification solution, it also appears transparent after plunging into liquid N_2 in the straw. Table 1 details the effect of various combinations of Fe_3O_4 nanoparticles, non-penetrating cryoprotectant (trehalose), and penetrating cryoprotectants (PROH and EG) on the vitrification of the solution in the straw. Fe_3O_4 nanoparticles did not facilitate the vitrification of the cryopreservation solution. However, with trehalose, ice formation is evitable to achieve vitrification.

We checked the effect of Fe_3O_4 nanoparticles on the survival of vitrified primary hUCM-MSCs. Figure 3b shows representative fluorescence micrographs of the hUCM-MSCs stained live/dead (AO/EB) fluorescence probes after rewarming the cells vitrified with various concentrations of Fe_3O_4 nanoparticles. Viability of fresh cells without cryopreservation without Fe_3O_4 nanoparticles was quantified using the same method. As expected, the viability of fresh cells was high, indicated by the bright green fluorescence of the AO dye with negligible red fluorescence of the EB dye (Figure 3b). However, hUCM-MSCs post-cryopreservation by vitrification either with or without the Fe_3O_4 nanoparticles were stained with the red fluorescence. Figure 3c shows that viabilities of the hUCM-MSCs post-cryopreservation in the absence (0%) and presence (0.01%, 0.05% and 0.1% (w/v)) of Fe_3O_4 nanoparticles are all below 40%. Although the average viability seems to decrease along with the increase of the concentration of the SPM nanoparticles, the decrease is not statistically significant. This suggests that the SPM nanoparticles alone (in the absence of

external AC magnetic field) have no apparent influences on the viability of hUCM-MSCs post cryopreservation by vitrification.

Effect of MIH with Fe_3O_4 nanoparticles on cryopreservation of primary hUCM-MSCs by vitrification

Figure 4a shows the representative fluorescence micrographs of hUCM-MSCs stained with live/dead dyes after cryopreservation by vitrification with and without MIH for rewarming. The corresponding quantitative data are shown in Figure 4b. MIH in an AC magnetic field with 0.01 and 0.1% (w/v) Fe_3O_4 nanoparticles slightly increased viability. More importantly, MIH in the same AC magnetic field with 0.05% (w/v) Fe_3O_4 nanoparticles during rewarming significantly improves the viability of hUCM-MSCs post-cryopreservation by vitrification.

To obtain optimal MIH condition for rewarming, we further investigated the effect of the electric current for MIH on the outcome of cryopreservation by vitrification. Figure 4c shows the typical two-channel (FITC-Annexin V and PI) flow cytometry data from current response experiments with quadrant gates showing four populations. The corresponding quantitative data from at least three independent runs are shown in Figure 4d. For the fresh cells without treatment as the positive control, the majority of cells were viable (91.3%, Annexin V^-/PI^-). In contrast, when cells vitrified with 2.0 M EG and 2.0 M PROH without MIH (0.05% (w/v) Fe_3O_4 nanoparticles) during rewarming, only 18.2% of cells (Annexin V^-/PI^-) survived. Moreover, with MIH during rewarming, there was a significant increase in the Annexin V^-/PI^- population and a corresponding decrease in cells that died of necrosis (Annexin V^-/PI^+) as shown in Figure 4d. The percentages of cells that died of apoptosis (Annexin V^+/PI^-) and both necrosis and apoptosis (Annexin V^+/PI^+) do not appear to be affected by the MIH during rewarming. Figure 4e shows the effect of the current for generating the magnetic field on the cell viability (i.e., percentage of Annexin V^-/PI^- hUCM-MSCs) post-cryopreservation by vitrification with 0.05% (w/v) Fe_3O_4 nanoparticles for MIH during rewarming. According to the FDA guidelines, cell viability should be > 70% for the release of cell therapy product lots [73]. Our approach are in compliance with the requirement, since we obtain 71.7% recovery of viable cells (Annexin V^-/PI^- hUCM-MSCs) if 0.05% (w/v) Fe_3O_4 nanoparticles were used together with MIH rewarming (15A, 375 kHz). Additionally, the cell viability of only one out of four times in our experiments falls below the FDA requirement for 70%, i.e., without further optimization, the likely failure rate of the MIH rewarming method is about 25%. Besides, A low current at 5 A may not enough to generate fast enough MIH heating to minimize devitrification/recrystallization induced cell death during rewarming and a current that is too high (e.g., > 30 A) may induce cell death by overheating the cells during rewarming.

We further examined the attachment efficiency of the cryopreserved hUCM-MSCs with MIH for rewarming (375 kHz, 10 s, and 0.05% (w/v) Fe_3O_4 nanoparticles). The attachment efficiency was calculated as the percentage of attached live cells post-cryopreservation relative to the number of fresh cells after 1 d of culture. As shown in Figure 4f, only 15% of the cells with cryopreservation without MIH during rewarming were able to attach on the dish. Moreover, the MIH for rewarming significantly improves the attachment efficiency of

the cells post-cryopreservation. Similar to the trend of cell viability, a slight decrease in attachment efficiency was observed as the current increases from 15 to 30 A. Moreover, the attached cells post-cryopreservation with MIH for rewarming proliferated similarly to fresh hUCM-MSCs (Figure 4g). The morphology of the hUCM-MSCs post-cryopreservation with MIH was also similar to that of fresh hUCM-MSCs after culture for up to 3 d (Figure S2). These data indicate that the MIH of Fe_3O_4 nanoparticles in an AC magnetic field can significantly augment recovery of cryopreservation by vitrification. SPM nanoparticles have zero magnetization once the applied magnetic field is removed and are unlikely to agglomerate, which makes them the ideal choice for enhancing both the rate and uniformity of heating cryopreserved sample during rewarming by acting as spatially uniformly dispersed point sources of heating upon exposure to external AC magnetic field [74, 75].

The hUCM-MSCs cryopreserved by vitrification with MIH for rewarming were observed by TEM and representative images are shown in Figure 5a. The cryopreserved cells exhibit similar ultra-structure as fresh cells with normal nuclear and cytoplasmic morphology. Distinct nuclei (indicated by the white arrow) were observable in both the fresh and cryopreserved cells, and apoptosis bodies were not present in the anisotropic nuclei. Moreover, the mitochondria and endoplasmic reticula are similar in the fresh and cryopreserved cells. These data indicate the hUCM-MSCs cryopreserved by vitrification with MIH for rewarming retain normal subcellular ultrastructure. In addition, no Fe_3O_4 nanoparticle is observed in the cells after cryopreservation.

To assess the functional survival of the hUCM-MSCs cryopreserved by vitrification with MIH for warming, we studied their stemness and capability of multi-lineage differentiation. As shown in Figure 5b, flow cytometry analyses indicate that the expression of two typical surface markers ($CD44^+$ and $CD31^-$) on the fresh and cryopreserved hUCM-MSCs is similar not significantly different. The data on adipogenic, osteogenic, and chondrogenic differentiations of the cryopreserved and fresh hUCM-MSCs are shown in Figure 5c. For adipogenic differentiation, no significance was observed between the two groups of cells in terms of Oil Red O staining of adipocyte-like cells with lipid-filled droplets. For osteogenic differentiation, both groups of cells maintained similar osteogenic potential assessed by Alizarin Red S staining of calcific deposition, a major function of osteoblasts. For chondrogenic differentiation, Alcian Blue staining of sulfated proteoglycan deposits that are indicative of the presence of functional chondrocytes is not significantly different between the fresh and cryopreserved hUCM-MSCs. These data indicate that the cryopreserved hUCM-MSCs retain their stemness and functional capability of multi-lineage differentiation.

It is worth noting that in this study, we demonstrated the MIH-enhanced vitrification approach using a single straw containing ~200 μL of cell suspension with ~2 million cells. For the eventual application of this approach to cryopreserve many more stem cells for clinical use, an inexpensive device that is compatible with the MIH technology should be further designed to allow for cryopreserving the cells using multiple straws in parallel. This work is ongoing in our laboratories.

Conclusions

In this study, we synthesized SPM Fe_3O_4 nanoparticles using the chemical coprecipitation method and thoroughly characterized their effect on cell cryopreservation by vitrification. It was found that the nanoparticles are highly compatible with minimal toxicity to the hUCM-MSCs. However, the Fe_3O_4 nanoparticles alone have no significant impact on the cryopreservation of hUCM-MSCs by vitrification. More importantly, the hUCM-MSCs can be used for MIH to improve the heating rate during rewarming of vitrified cells to significantly improve the post-vitrification survival of the hUCM-MSCs. Moreover, the cells retain their stemness and functional capability of multi-lineage differentiation after cryopreservation by vitrification using an optimized protocol with Fe_3O_4 nanoparticle-mediate MIH during rewarming. Our results indicate that utilizing Fe_3O_4 nanoparticles for MIH during rewarming is a promising strategy for advancing cryopreservation of hUCM-MSCs and possibly many other important cells by vitrification to meet their ever increasing demand by the burgeoning cell-based medicine.

Supplementary Material

Refer to Web version on PubMed Central for supplementary material.

Acknowledgments

This work was partially supported by grants from NSFC (Nos. 51276179, 51476160 and 51528601). X.H. was funded by grants from NSF (CBET-1154965) and NIH (R01EB012108).

Appendix A. Supplementary data

Figure S1 presents pictures of straws and the magnetic induction heating apparatus, and Figure S2 shows the morphology of fresh and cryopreserved hUCM-MSCs. The data can be found in supplementary material.

References

1. Pittenger MF, Mackay AM, Beck SC, Jaiswal RK, Douglas R, Mosca JD, et al. Multilineage potential of adult human mesenchymal stem cells. Science. 1999; 284:143–7. [PubMed: 10102814]
2. Caplan AI, Bruder SP. Mesenchymal stem cells: building blocks for molecular medicine in the 21st century. Trends Mol Med. 2001; 7:259–64. [PubMed: 11378515]
3. Divya MS, Roshin GE, Divya TS, Rasheed VA, Santhoshkumar TR, Elizabeth KE, et al. Umbilical cord blood-derived mesenchymal stem cells consist of a unique population of progenitors co-expressing mesenchymal stem cell and neuronal markers capable of instantaneous neuronal differentiation. Stem Cell Res Ther. 2012; 3:57. [PubMed: 23253356]
4. Fox IJ, Daley GQ, Goldman SA, Huard J, Kamp TJ, Trucco M. Use of differentiated pluripotent stem cells in replacement therapy for treating disease. Science. 2014; 345
5. Chang YJ, Tseng CP, Hsu LF, Hsieh TB, Hwang SM. Characterization of two populations of mesenchymal progenitor cells in umbilical cord blood. Cell Biol Int. 2006; 30:495–9. [PubMed: 16731010]
6. Troyer DL, Weiss ML. Wharton's jelly-derived cells are a primitive stromal cell population. Stem Cells. 2008; 26:591–9. [PubMed: 18065397]
7. Caplan AI. Why are MSCs therapeutic? New data: new insight. J Pathol. 2009; 217:318–24. [PubMed: 19023885]

8. Le Blanc K, Tammik L, Sundberg B, Haynesworth SE, Ringden O. Mesenchymal stem cells inhibit and stimulate mixed lymphocyte cultures and mitogenic responses independently of the major histocompatibility complex. Scand J Immunol. 2003; 57:11–20. [PubMed: 12542793]
9. Weiss ML, Medicetty S, Bledsoe AR, Rachakatla RS, Choi M, Merchav S, et al. Human umbilical cord matrix stem cells: preliminary characterization and effect of transplantation in a rodent model of Parkinson's disease. Stem Cells. 2006; 24:781–92. [PubMed: 16223852]
10. Buzhor E, Leshansky L, Blumenthal J, Barash H, Warshawsky D, Mazor Y, et al. Cell-based therapy approaches: the hope for incurable diseases. Regen Med. 2014; 9:649–72. [PubMed: 25372080]
11. King NM, Perrin J. Ethical issues in stem cell research and therapy. Stem Cell Res Ther. 2014; 5:85. [PubMed: 25157428]
12. Hunt CJ. Cryopreservation of Human Stem Cells for Clinical Application: A Review. Transfusion Medicine and Hemotherapy. 2011; 38:107–23. [PubMed: 21566712]
13. Langer R, Vacanti J. Tissue engineering. Science. 1993; 260:920–6. [PubMed: 8493529]
14. Blow N. Biobanking: freezer burn. Nat Meth. 2009; 6:173–8.
15. Pancrazio JJ, Wang F, Kelley CA. Enabling tools for tissue engineering. Biosensors and Bioelectronics. 2007; 22:2803–11. [PubMed: 17240132]
16. Marquez-Curtis LA, Janowska-Wieczorek A, McGann LE, Elliott JA. Mesenchymal stromal cells derived from various tissues: Biological, clinical and cryopreservation aspects. Cryobiology. 2015; 71:181–97. [PubMed: 26186998]
17. Liem IK, Goei N, Pawitan JA, Mediana D. Effect of Platelet Rich Plasma on Post Cryopreservation Viability, Morphology and Proliferation of Human Umbilical Cord Stem Cells. OnLine Journal of Biological Sciences. 2015; 15:42–8.
18. Yang G, Veres M, Szalai G, Zhang A, Xu LX, He X. Biotransport phenomena in freezing mammalian oocytes. Annals of biomedical engineering. 2011; 39:580–91. [PubMed: 20848315]
19. Fahy GM, MacFarlane DR, Angell CA, Meryman HT. Vitrification as an approach to cryopreservation. Cryobiology. 1984; 21:407–26. [PubMed: 6467964]
20. Huang H, Choi JK, Rao W, Zhao S, Agarwal P, Zhao G, et al. Alginate hydrogel microencapsulation inhibits devitrification and ice recrystallization and enables large-volume low-CPA cell vitrification. Advanced Functional Materials. 2015; 25:6839–50.
21. Choi JK, Huang H, He X. Improved low-CPA vitrification of mouse oocytes using quartz microcapillary. Cryobiology. 2015; 70:269–72. [PubMed: 25869750]
22. Choi JK, Yue T, Huang H, Zhao G, Zhang M, He X. The crucial role of zona pellucida in cryopreservation of oocytes by vitrification. Cryobiology. 2015; 71:350–5. [PubMed: 26297946]
23. Seki S, Jin B, Mazur P. Extreme rapid warming yields high functional survivals of vitrified 8-cell mouse embryos even when suspended in a half-strength vitrification solution and cooled at moderate rates to −196 degrees C. Cryobiology. 2014; 68:71–8. [PubMed: 24333434]
24. Peyridieu JF, Baudot A, Boutron P, Mazuer J, Odin J, Ray A, et al. Critical cooling and warming rates to avoid ice crystallization in small pieces of mammalian organs permeated with cryoprotective agents. Cryobiology. 1996; 33:436–46. [PubMed: 8764852]
25. Rall WF, Fahy GM. Ice-free cryopreservation of mouse embryos at −196 degrees C by vitrification. Nature. 1985; 313:573–5. [PubMed: 3969158]
26. He X, Park EY, Fowler A, Yarmush ML, Toner M. Vitrification by ultra-fast cooling at a low concentration of cryoprotectants in a quartz micro-capillary: a study using murine embryonic stem cells. Cryobiology. 2008; 56:223–32. [PubMed: 18462712]
27. Berejnov V, Husseini NS, Alsaied OA, Thorne RE. Effects of cryoprotectant concentration and cooling rate on vitrification of aqueous solutions. Journal of Applied Crystallography. 2006; 39:244–51.
28. Jacobsen IA, Pegg DE, Starklint H, Chemnitz J, Hunt C, Barfort P, et al. Effect of cooling and warming rate on glycerolized rabbit kidneys. Cryobiology. 1984; 21:637–53. [PubMed: 6394215]
29. Karlsson JO, Toner M. Long-term storage of tissues by cryopreservation: critical issues. Biomaterials. 1996; 17:243–56. [PubMed: 8745321]

30. Etheridge ML, Xu Y, Rott L, Choi J, Glasmacher B, Bischof JC. RF heating of magnetic nanoparticles improves the thawing of cryopreserved biomaterials. TECHNOLOGY. 2014; 02:229–42.
31. Robinson MP, Pegg DE. Rapid electromagnetic warming of cells and tissues. IEEE Trans Biomed Eng. 1999; 46:1413–25. [PubMed: 10612899]
32. Ruggera PS, Fahy GM. Rapid and uniform electromagnetic heating of aqueous cryoprotectant solutions from cryogenic temperatures. Cryobiology. 1990; 27:465–78. [PubMed: 2249450]
33. Guttman FM, Lizin J, Robitaille P, Blanchard H, Turgeon-Knaack C. Survival of canine kidneys after treatment with dimethyl-sulfoxide, freezing at −80 degrees C, and thawing by microwave illumination. Cryobiology. 1977; 14:559–67. [PubMed: 332449]
34. Ketterer FD, Holst HI, Lehr HB. Improved viability of kidneys with microwave thawing. Cryobiology. 1971; 8:395.
35. Pegg DE, Green CJ, Walter CA. Attempted canine renal cryopreservation using dimethyl sulphoxide helium perfusion and microwave thawing. Cryobiology. 1978; 15:618–26. [PubMed: 369772]
36. Ruggera PS, Fahy GM. Rapid and uniform electromagnetic heating of aqueous cryoprotectant solutions from cryogenic temperatures. Cryobiology. 1990; 27:465–78. [PubMed: 2249450]
37. Robinson MP, Wusteman MC, Wang L, Pegg DE. Electromagnetic re-warming of cryopreserved tissues: effect of choice of cryoprotectant and sample shape on uniformity of heating. Phys Med Biol. 2002; 47:2311–25. [PubMed: 12164589]
38. Luo D, Yu C, He L, Lu C, Gao D. Development of a single mode electromagnetic resonant cavity for rewarming of cryopreserved biomaterials. Cryobiology. 2006; 53:288–93. [PubMed: 16930581]
39. Jin B, Kleinhans FW, Mazur P. Survivals of mouse oocytes approach 100% after vitrification in 3-fold diluted media and ultra-rapid warming by an IR laser pulse. Cryobiology. 2014; 68:419–30. [PubMed: 24662030]
40. Kleinhans FW, Mazur P. Physical parameters, modeling, and methodological details in using IR laser pulses to warm frozen or vitrified cells ultra-rapidly. Cryobiology. 2015; 70:195–203. [PubMed: 25724528]
41. Jin B, Mazur P. High survival of mouse oocytes/embryos after vitrification without permeating cryoprotectants followed by ultra-rapid warming with an IR laser pulse. Scientific Reports. 2015; 5:9271. [PubMed: 25786677]
42. Pankhurst QA, Connolly J, Jones SK, Dobson J. Applications of magnetic nanoparticles in biomedicine. Journal of Physics D: Applied Physics. 2003; 36:R167.
43. Mornet S, Vasseur S, Grasset F, Duguet E. Magnetic nanoparticle design for medical diagnosis and therapy. Journal of Materials Chemistry. 2004; 14:2161–75.
44. Lai B-H, Chen D-H. Vancomycin-modified LaB6@SiO2/Fe3O4 composite nanoparticles for near-infrared photothermal ablation of bacteria. Acta Biomaterialia. 2013; 9:7573–9. [PubMed: 23535232]
45. Zhu A, Yuan L, Jin W, Dai S, Wang Q, Xue Z, et al. Polysaccharide surface modified Fe3O4 nanoparticles for camptothecin loading and release. Acta Biomaterialia. 2009; 5:1489–98. [PubMed: 19286431]
46. Schildkopf P, Ott OJ, Frey B, Wadepohl M, Sauer R, Fietkau R, et al. Biological rationales and clinical applications of temperature controlled hyperthermia–implications for multimodal cancer treatments. Curr Med Chem. 2010; 17:3045–57. [PubMed: 20629627]
47. Zhao L, Yang B, Wang Y, Yao Z, Wang X, Feng SS, et al. Thermochemotherapy mediated by novel solar-planet structured magnetic nanocomposites for glioma treatment. J Nanosci Nanotechnol. 2012; 12:1024–31. [PubMed: 22629888]
48. Xu C, Zheng Y, Gao W, Xu J, Zuo G, Chen Y, et al. Magnetic Hyperthermia Ablation of Tumors Using Injectable Fe3O4/Calcium Phosphate Cement. ACS Applied Materials & Interfaces. 2015; 7:13866–75. [PubMed: 26065316]
49. Sadhukha T, Niu L, Wiedmann TS, Panyam J. Effective Elimination of Cancer Stem Cells by Magnetic Hyperthermia. Molecular Pharmaceutics. 2013; 10:1432–41. [PubMed: 23432410]

50. Kruse AM, Meenach SA, Anderson KW, Hilt JZ. Synthesis and characterization of CREKA-conjugated iron oxide nanoparticles for hyperthermia applications. Acta Biomaterialia. 2014; 10:2622–9. [PubMed: 24486913]
51. Wang T, Zhao G, Liang XM, Xu Y, Li Y, Tang H, et al. Numerical simulation of the effect of superparamagnetic nanoparticles on microwave rewarming of cryopreserved tissues. Cryobiology. 2014; 68:234–43. [PubMed: 24530372]
52. Yan JF, Liu J. Nanocryosurgery and its mechanisms for enhancing freezing efficiency of tumor tissues. Nanomedicine. 2008; 4:79–87. [PubMed: 18155645]
53. Willard MA, Kurihara LK, Carpenter EE, Calvin S, Harris VG. Chemically prepared magnetic nanoparticles. Int Mater Rev. 2004; 49:125–70.
54. Simoes IN, Boura JS, dos Santos F, Andrade PZ, Cardoso CM, Gimble JM, et al. Human mesenchymal stem cells from the umbilical cord matrix: successful isolation and ex vivo expansion using serum-/xeno-free culture media. Biotechnol J. 2013; 8:448–58. [PubMed: 23420807]
55. Leite C, Silva NT, Mendes S, Ribeiro A, de Faria JP, Lourenco T, et al. Differentiation of human umbilical cord matrix mesenchymal stem cells into neural-like progenitor cells and maturation into an oligodendroglial-like lineage. PLoS One. 2014; 9:e111059. [PubMed: 25357129]
56. Kalambur VS, Longmire EK, Bischof JC. Cellular level loading and heating of superparamagnetic iron oxide nanoparticles. Langmuir. 2007; 23:12329–36. [PubMed: 17960940]
57. Fish WW. Rapid colorimetric micromethod for the quantitation of complexed iron in biological samples. Methods Enzymol. 1988; 158:357–64. [PubMed: 3374387]
58. Kuddannaya S, Chuah YJ, Lee MH, Menon NV, Kang Y, Zhang Y. Surface chemical modification of poly(dimethylsiloxane) for the enhanced adhesion and proliferation of mesenchymal stem cells. ACS Appl Mater Interfaces. 2013; 5:9777–84. [PubMed: 24015724]
59. Rao W, Huang H, Wang H, Zhao S, Dumbleton J, Zhao G, et al. Nanoparticle-mediated intracellular delivery enables cryopreservation of human adipose-derived stem cells using trehalose as the sole cryoprotectant. ACS Appl Mater Interfaces. 2015; 7:5017–28. [PubMed: 25679454]
60. Wahajuddin, Arora S. Superparamagnetic iron oxide nanoparticles: magnetic nanoplatforms as drug carriers. Int J Nanomedicine. 2012; 7:3445–71. [PubMed: 22848170]
61. Trindade, T., da Silva, ALD. Nanocomposite particles for bio-applications: materials and bio-interfaces. CRC Press; 2011.
62. Conner SD, Schmid SL. Regulated portals of entry into the cell. Nature. 2003; 422:37–44. [PubMed: 12621426]
63. Verma A, Stellacci F. Effect of surface properties on nanoparticle-cell interactions. Small. 2010; 6:12–21. [PubMed: 19844908]
64. Guha A, Devireddy R. Effect of Palmitoyl Nanogold Particles on the Subzero Thermal Properties of Phosphate Buffered Saline Solutions. Journal of Nanotechnology in Engineering and Medicine. 2010; 1:021004.
65. Han X, Ma H, Wilson C, Critser J. Effects of nanoparticles on the nucleation and devitrification temperatures of polyol cryoprotectant solutions. Microfluidics and nanofluidics. 2008; 4:357–61.
66. Lv F, Liu B, Li W, Jaganathan GK. Devitrification and recrystallization of nanoparticle-containing glycerol and PEG-600 solutions. Cryobiology. 2014; 68:84–90. [PubMed: 24374134]
67. Lv F, Liu B, Li W, Song X. Effects of nanoparticles on devitrification and recrystallization of aqueous glycerol and PEG-600 solutions. Sci China Technol Sci. 2014; 57:264–9.
68. Zhou X, Li W, Zhang D, Dai J. Hydroxyapatite nanoparticles improved survival rate of vitrified porcine oocytes and its mechanism. Cryo Letters. 2015; 36:45–50. [PubMed: 26017172]
69. Sun WQ, Leopold AC, Crowe LM, Crowe JH. Stability of dry liposomes in sugar glasses. Biophys J. 1996; 70:1769–76. [PubMed: 8785336]
70. He X. Thermostability of biological systems: fundamentals, challenges, and quantification. Open Biomed Eng J. 2011; 5:47–73. [PubMed: 21769301]
71. Zhang W, Yang G, Zhang A, Xu LX, He X. Preferential vitrification of water in small alginate microcapsules significantly augments cell cryopreservation by vitrification. Biomed Microdevices. 2010; 12:89–96. [PubMed: 19787454]

72. Eroglu A, Russo MJ, Bieganski R, Fowler A, Cheley S, Bayley H, et al. Intracellular trehalose improves the survival of cryopreserved mammalian cells. Nat Biotechnol. 2000; 18:163–7. [PubMed: 10657121]

73. CBER. Administration UFaD. Rockville: 2008. Guidance for FDA Reviewers and Sponsors: Content and Review of Chemistry, Manufacturing, and Control (CMC) Information for Human Somatic Cell Therapy Investigational New Drug Applications (INDs).

74. Dave SR, Gao X. Monodisperse magnetic nanoparticles for biodetection, imaging, and drug delivery: a versatile and evolving technology. Wiley Interdiscip Rev Nanomed Nanobiotechnol. 2009; 1:583–609. [PubMed: 20049819]

75. Jordan A, Scholz R, Wust P, Fähling H, Roland F. Magnetic fluid hyperthermia (MFH): Cancer treatment with AC magnetic field induced excitation of biocompatible superparamagnetic nanoparticles. Journal of Magnetism and Magnetic Materials. 1999; 201:413–9.

Statement of Significance

In this manuscript, we report the successful synthesis and application of Fe_3O_4 nanoparticles for magnetic induction heating (MIH) to enhance rewarming of vitrification-cryopreserved human umbilical cord matrix mesenchymal stem cells (hUCM-MSCs). We found that MIH-enhanced rewarming greatly improves the survival of vitrification-cryopreserved hUCM-MSCs. Moreover, the hUCM-MSCs retain their intact stemness and multilineage potential of differentiation post cryopreservation by vitrification with the MIH-enhanced rewarming. Therefore, the novel MIH-enhanced cell vitrification is valuable to facilitate the long-term storage of adult stem cells to meet their ever-increasing demand by the burgeoning cell-based medicine.

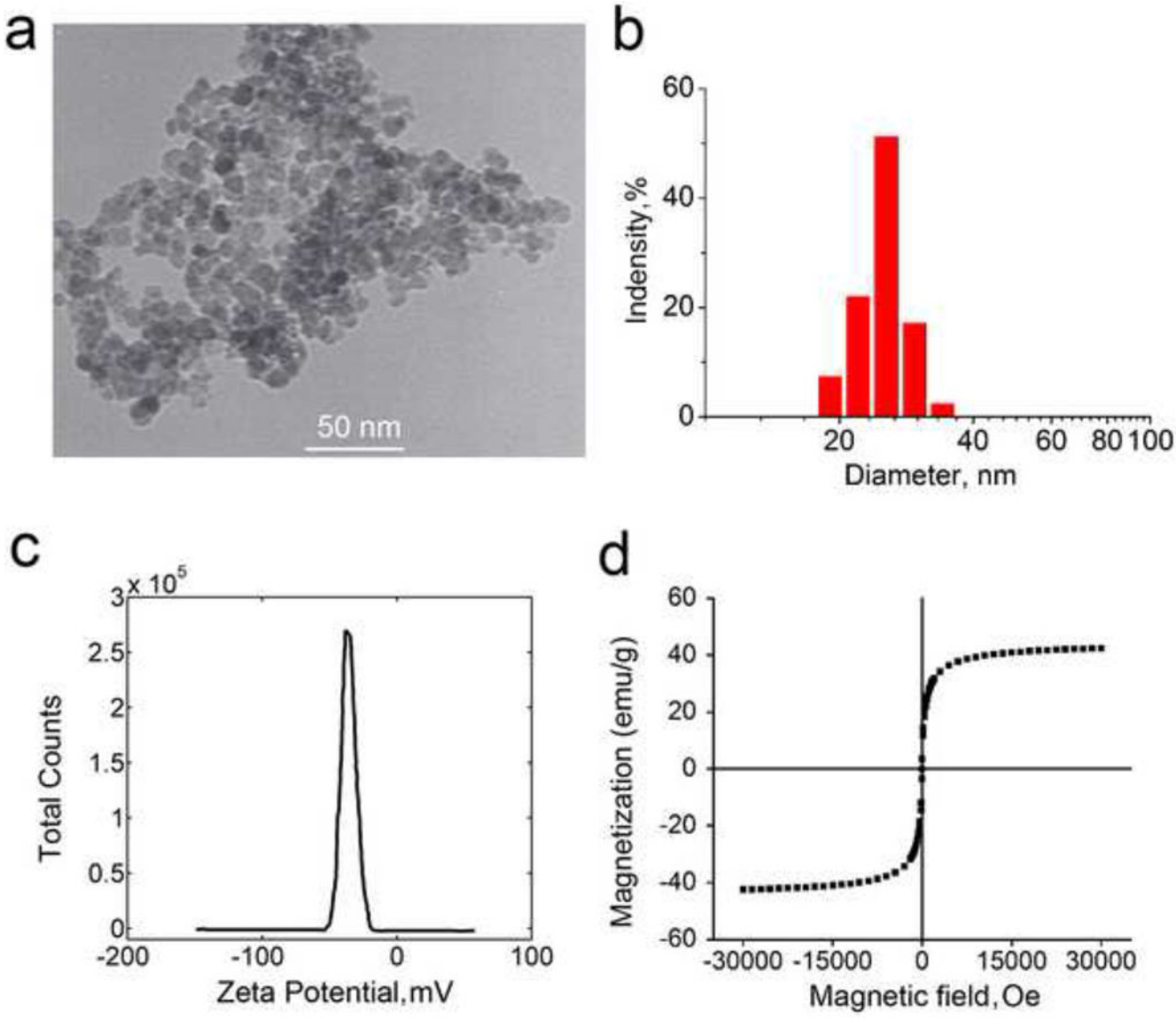

Figure 1.

Characterization of coprecipitation synthesized Fe_3O_4 nanoparticles: (a) Representative TEM image of Fe_3O_4 nanoparticles showing their morphology and size; (b) Size distribution of Fe_3O_4 nanoparticles determined by dynamic light scattering at room temperature; (c) Zeta potential of Fe_3O_4 nanoparticles measured at room temperature; and (d) Vibrating sample magnetometer measurement showing the magnetic property of the nanoparticles.

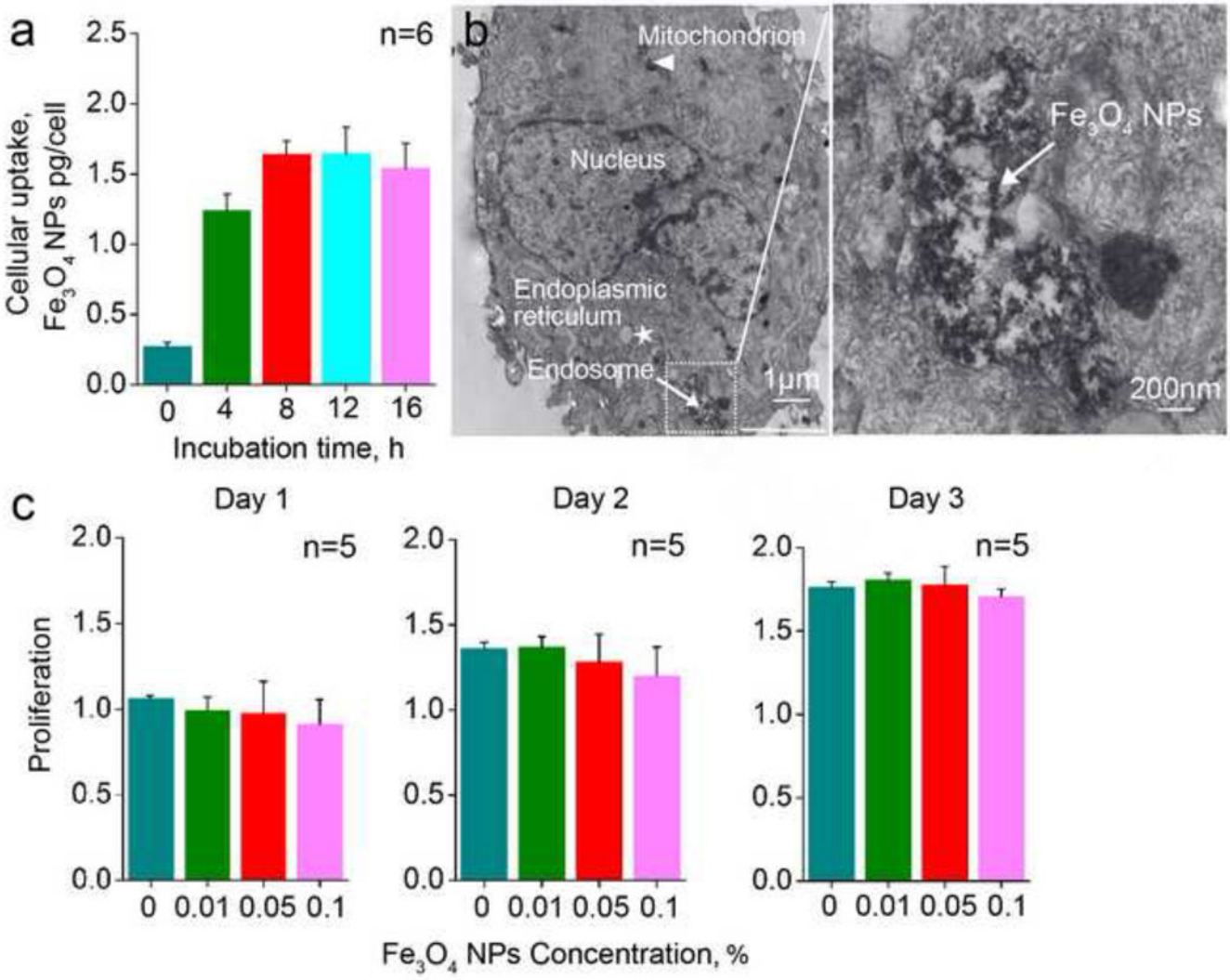

Figure 2.

Cell uptake and cytotoxicity of Fe_3O_4 nanoparticles: (a) Fe_3O_4 nanoparticles in the hUCM-MSCs after incubation for different time determined using the colorimetric assay; (b) Representative TEM images of the hUCM-MSCs incubated with Fe_3O_4 nanoparticles for 12 h. (c) Proliferation of the hUCM-MSCs after incubating with Fe_3O_4 nanoparticles at varying concentrations (0, 0.01, 0.05, and 0.1% (w/v)) for 1, 2, and 3 days. Here, proliferation is defined as the number of cells cultured with various concentrations of Fe_3O_4 nanoparticles for various days normalized to the number of the cells cultured in medium without the nanoparticle on day 1.

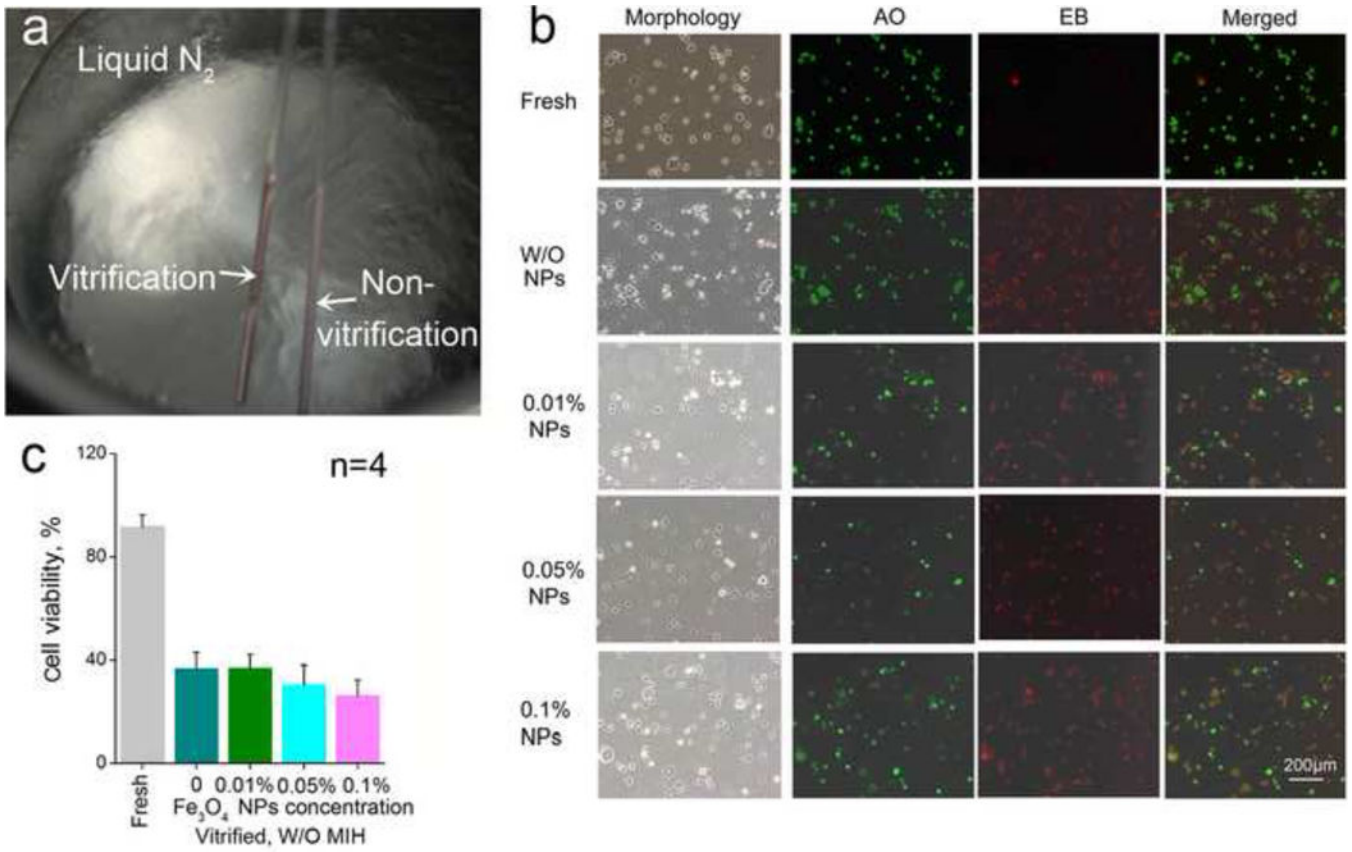

Figure 3.

Effect of Fe_3O_4 nanoparticles on cryopreservation by vitrification: (a) The different appearances of the solutions in straws plunged into liquid N_2 with the non-vitrified solution being whitish as a result of ice formation; (b) Phase and fluorescence micrographs of hUCM-MSCs vitrified with varying concentrations of Fe_3O_4 nanoparticles in the vitrification solution; and (c) Quantitative viability data of the hUCM-MSCs after cryopreservation by vitrification.

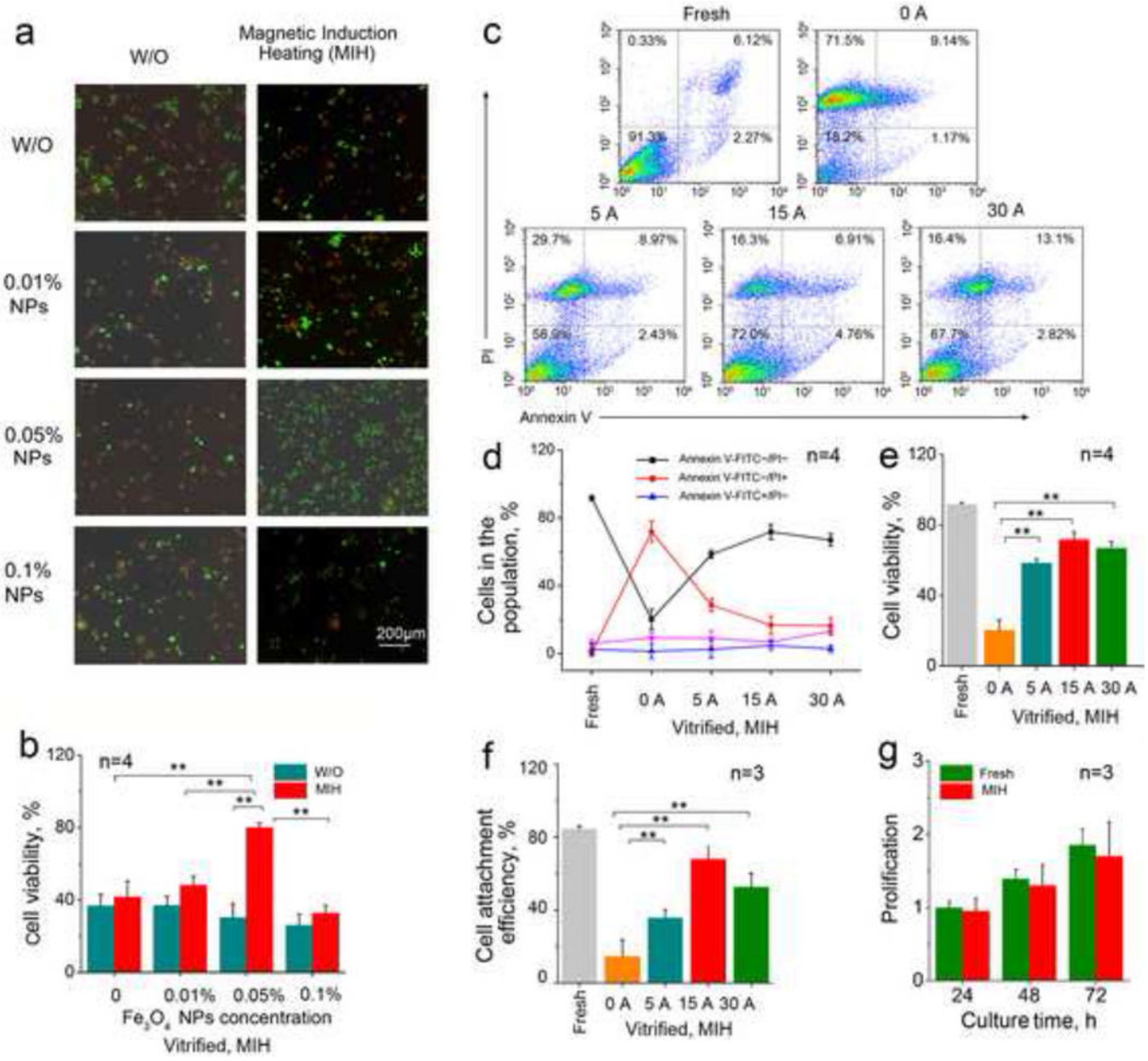

Figure 4.

Magnetic induction heating (MIH) with Fe_3O_4 nanoparticles in an AC magnetic field improves the viability of hUCM-MSCs post-cryopreservation by vitrification: (a) Representative fluorescence micrographs showing live (green) and dead (read) staining of hUCM-MSCs post-cryopreservation by vitrification with and without MIH during rewarming; (b) Quantitative data of the viability of hUCM-MSCs post-cryopreservation by vitrification with and without MIH during rewarming. (c) Typical two-channel flow cytometry data (Annexin V-FITC and PI double staining), (d) quantitative data of different cell populations from the flow cytometry analysis, (e) cell viability calculated as the percentage of cells with negative staining of both Annexin V and PI, and (f) Attachment efficiency of the hUCM-MSCs after cryopreservation by vitrification with MIH (0.05%

(w/v) Fe_3O_4 nanoparticles) at the different currents during rewarming; (g) Proliferation of fresh hUCM-MSCs and the cells cryopreserved by vitrification with MIH (15 A and 0.05% (w/v) Fe_3O_4 nanoparticles) during rewarming. *, $p < 0.05$; **, $p < 0.01$.

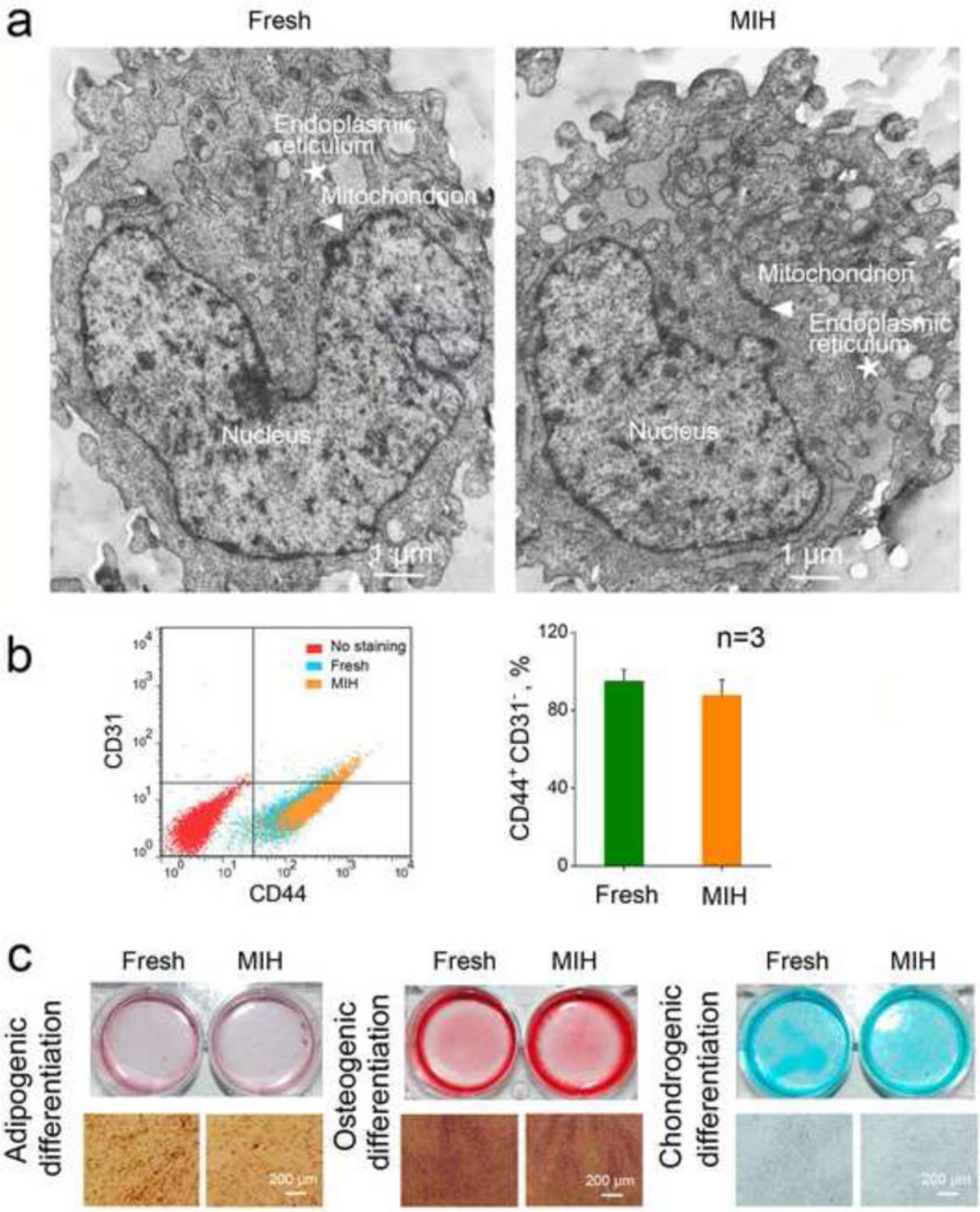

Figure 5.

The hUCM-MSCs cryopreserved by vitrification with MIH for rewarming retain the subcellular ultra-structure, stemness, and capability of multi-lineage differentiation: (a) Representative TEM image of fresh and post-cryopreserved hUCM-MSCs. The arrowhead and star represent mitochondria and endoplasmic reticulum, respectively; (b) Comparable expression of CD44+ and CD31− on fresh and cryopreserved hUCM-MSCs; and (c) Adipogenic, osteogenic, and chondrogenic differentiations of fresh and cryopreserved

hUCM-MSCs indicated by Oil Red O stain of lipid-filled droplets, Alizarin Red S stain of calcific depositions, and Alcian Blue stain of sulfated proteoglycan.

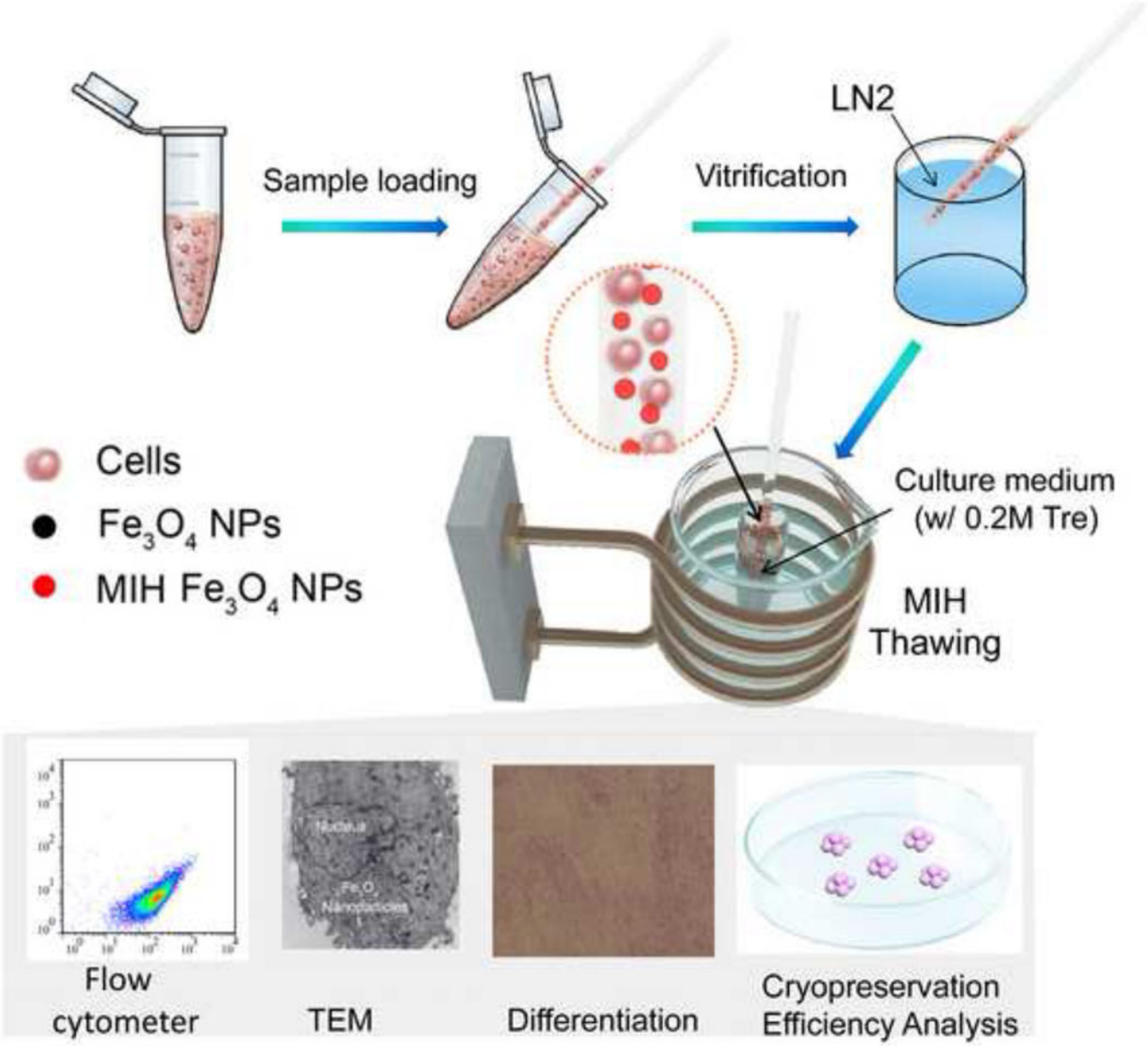

Scheme 1.

A schematic illustration of the procedure for hUCM-MSC cryopreservation with magnetic induction heating (MIH). LN2: liquid nitrogen; NPs: nanoparticles; Tre: trehalose.

Table 1

Effects of Fe_3O_4 nanoparticles and cryoprotectant solution in the straw on the vitrified cryopreservation.

Trehalose	Fe_3O_4 NPs	PROH:EG (1:1)		
		1.0 M	1.5 M	2.0 M
W/O	W/O	−	−	+
	W	−	−	−
0.5 M	W/O	−	−	+
	W	−	−	+
1.0 M	W/O	−	−/+	+
	W	−	−	+

The symbols + and − represent apparent vitrification and appearance of visible ice crystal (opacity) in the whole solution volume, respectively. The symbol "−/+" indicates partial apparent vitrification.